Tellus (1994), 46A, 134–148
Printed in Belgium – all rights reserved

TELLUS
ISSN 0280–6495

An analysis of the vertical velocity field computed by a three-dimensional model in the region of the Bering Strait

By ERIC DELEERSNIJDER, *G. Lemaître Institute of Astronomy and Geophysics (ASTR), 2, Chemin du Cyclotron, Catholic University of Louvain, B-1348 Louvain-la-Neuve, Belgium*

(Manuscript received 8 October 1992; in final form 28 June 1993)

ABSTRACT

The main features of the general circulation in the region of the Bering Strait are summarized. This flow has been simulated by a three-dimensional hydrodynamic model, which is briefly described with some emphasis on the initial and boundary conditions. The modelled vertical velocity field is analysed. First, it is suggested to regard the vertical velocity as the sum of two components, namely the upsloping and the upwelling velocity. Next, the fields of upwelling and upsloping velocity are examined and it is seen that the vertical motions predicted by the model are qualitatively in agreement with the existence of a cold water plume downstream of the Anadyr Strait. Finally, a successful attempt is made to explain the upwelling phenomena found in the model results by a mechanism which relies on the velocity veering induced by the bottom stress, is independent of wind forcing, and is inspired by the classical theory of Ekman pumping.

1. Introduction

The Pacific and Arctic Oceans exchange mass, momentum, and energy through the Bering Strait only. The region of the Bering Strait exhibits some of the most intense biological productivity ever measured in the sea (Sambrotto et al., 1984; Whitledge et al., 1988; Walsh et al., 1989b), with peak values that can be of order 10^{-2} kg C m^{-2} day^{-1}. From a physical and biological point of view, the region of the Bering Strait is thus of high importance. This is why the U.S. National Science Foundation decided to set up, in the eighties, the Inner SHelf Transfer And Recycling (ISHTAR) programme, the aim of which was to study the ecohydrodynamics of the shallow seas surrounding the Bering Strait (Fig. 1). ISHTAR concentrated on the summer period, where the sea-ice cover may be neglected (Walsh et al., 1989a).

In the framework of ISHTAR, an extensive field survey of the domain of interest was achieved and numerous model results were produced. Some of them will be discussed here.

ISHTAR's hydrodynamic studies were carried out in an ecological perspective. Thus, it was deemed appropriate to devote most of the attention to the general circulation, i.e., the flow averaged over a sufficiently long time, say one week to one month, so that the meso-scale processes are filtered out. It is worth stressing that, in the domain of interest, the general circulation is associated with much of the kinetic energy (Aagaard et al., 1985; Coachman, 1986; Mofjeld, 1986; Walsh et al., 1989b), in marked contrast to what is observed in most shelf seas.

The monthly flow through the Bering Strait is directed to the North, i.e., from the Pacific to the Arctic. This flow is subject to an annual cycle reaching, during the summer months, a maximum that slightly exceeds 1 Sv (Coachman and Aagaard, 1988; Walsh et al., 1989b). Since Coachman and Aagaard (1966), it seems clear that the northward flow through the Bering Strait is primarily induced by the water level difference between the Pacific and the Arctic, which is attributed to a salinity contrast (Stigebrandt, 1984). It is believed that the variability of the flow mainly results from the wind forcing (Coachman et al., 1975; Aagaard et al., 1985; Coachman and Aagaard, 1988).

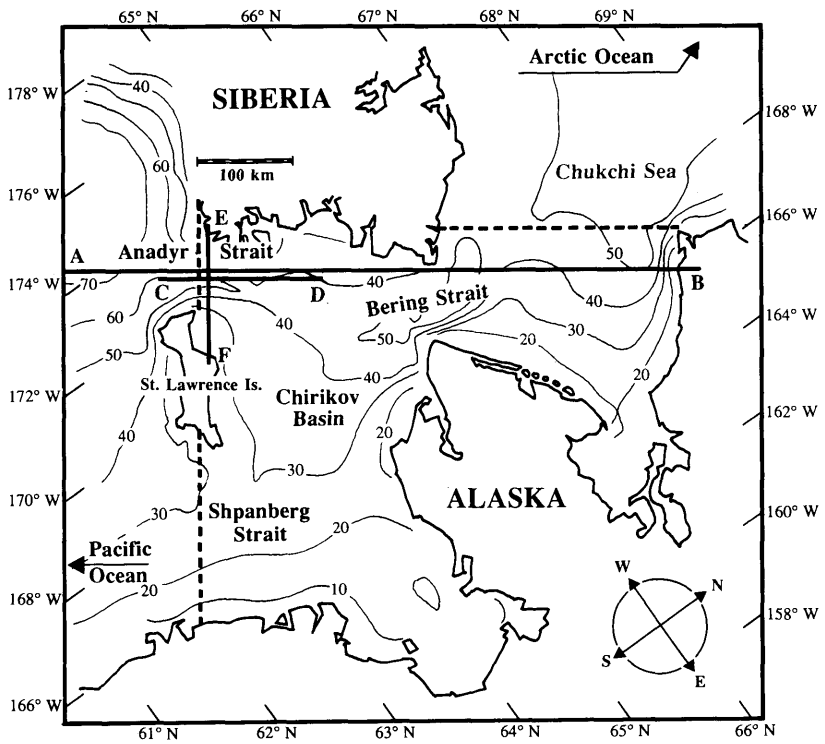

Fig. 1. Bathymetry of the computational domain, with depth in meters. The dashed lines indicate the limits of the domain of interest of ISHTAR. Lines AB, CD, and EF are related to the vertical sections shown in Figs. 3, 5, and 9, respectively.

Kinder et al. (1986) convincingly showed that β-bathymetric effect is responsible for the currents being more intense along the southern and western boundaries of the Bering Shelf. Accordingly, most of the water that finally crosses the Bering Strait originates from the Bering Slope Current, a branch of which enters the Gulf of Anadyr before going through the Anadyr Strait and the Shpanberg Strait. Two thirds of the northward flow passes through the Anadyr Strait (Coachman et al., 1975).

In the domain of interest the salinity gradient is predominantly horizontal, whereas the temperature contrasts are mostly observed along the vertical direction, with a marked thermocline (Coachman et al., 1975). Satellites infra-red pictures, displayed in Nihoul (1986), Nihoul et al. (1989), Walsh et al. (1989b), Deleersnijder (1992), show that a plume of cold water originates in the Anadyr Strait, near the Siberian coast. Although its extent depends on meso-scale hydrodynamic features, the cold water plume seems to be permanent, with an area of about 40×100 km^2 (Fig. 2).

All in situ temperature data collected by ISHTAR cruises and by the 1988 Soviet-American expedition aboard the Akademik Korolev have been analysed with the help of a sophisticated

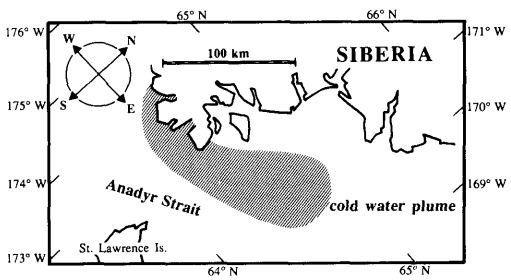

Fig. 2. Schematic shape of the surface plume of cold water downstream of the Anadyr Strait.

interpolation tool, named "Variational Inverse Model" (Brasseur, 1991; Brasseur and Haus, 1991; Haus, 1991). This work confirmed the existence of a plume of cold water downstream of the Anadyr Strait, indicated its persistence throughout the summer and suggested that an intense upwelling takes place in the "Siberian half" of the Anadyr Strait (Fig. 3). The Anadyr upwelling continuously brings nutrient from the lower layer to the euphotic zone, fueling the enormous primary production of the Anadyr stream (Nihoul, 1986; Walsh et al., 1989b; Coachman and Shigaev, 1992).

No device is able to directly measure vertical fluxes at reasonable cost. Moreover, indirect methods for estimating the magnitude of vertical motions from scalar data are known not to be very accurate. This pointed to the need for a three-dimensional hydrodynamic model to compute the vertical fluxes in the domain of interest.

Several two-dimensional models have been applied to the Northern Bering/Southern Chukchi Seas (Walsh and Dieterle, 1986; Overland and Roach, 1987; Spaulding et al., 1987; Brasseur, 1991). Although these models achieved appreciable realism in the representation of the horizontal motions, they did not provide any information about the vertical fluxes.

The pioneering three-dimensional modelling efforts of Liu and Leendertse, presented in an excellent report (Liu and Leendertse, 1987), were not conducted in an ecological perspective. Furthermore, the numerical grid used is probably too coarse for the upwelling zones to be realistically represented.

In the scope of ISHTAR, the Geo-Hydrodynamics and Environment Research (GHER) laboratory of the University of Liège undertook the three-dimensional modelling of the domain of interest with the aim of determining the up- and downwelling areas. Preliminary results were produced by Waleffe (1985) and Nihoul et al. (1986). A numerical simulation that was deemed to reasonably well estimate the location of the zones of strong vertical velocity was carried out somewhat later and reported in Deleersnijder and Nihoul (1988a, 1988b), Deleersnijder (1989), Nihoul et al. (1989), Walsh et al. (1989b), Deleersnijder (1992), and Nihoul et al. (1993).

In the present paper, one first outlines the version of GHER's 3-D model used in the region of the Bering Strait. Then, a method for analysing the vertical velocity field is described and applied to the results of the numerical simulation mentioned above. Finally, a mechanism is suggested that could account for the up- and downwellings in the region of the Bering Strait.

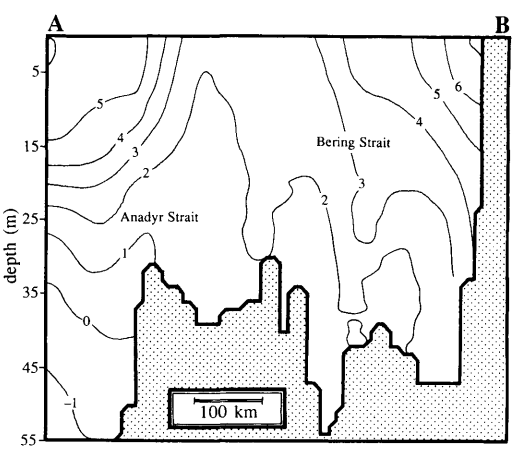

Fig. 3. Vertical section showing the temperature (°C) field reconstructed from all ISHTAR data by the variational inverse model. The plane of section AB passes through the Anadyr Strait and the Bering Strait, as indicated in Fig. 1. (Courtesy of J. Haus).

2. Model set-up

The equations of GHER's three-dimensional marine model have been established in Nihoul (1984), Nihoul and Djenidi (1987), Beckers (1991) and Deleersnijder (1992). All details about the application of this model to the region of the Bering Strait, including the numerics, are given in Deleersnijder (1992). However, a brief summary of this description is provided below.

The Boussinesq approximation and the hydrostatic equilibrium underlie GHER's 3-D model. The independent variables are time and the three space coordinates. The horizontal velocity, the temperature, the salinity and the sea surface elevation are computed from evolution equations. The continuity equation permits the determination of the vertical velocity while the density is derived from an appropriate equation of state, which can be found in Deleersnijder (1992). A turbulence closure model is called on to evaluate the vertical

eddy viscosity and diffusivity: each eddy coefficient is expressed as the product of a velocity scale and a length scale. The former is given by the square root of the turbulent kinetic energy, obtained from an evolution equation as in most turbulence closures (Mellor and Yamada, 1982; Rodi, 1987). The length scale is derived from an algebraic empirical formula taking into account the distance to the sea surface/bottom and the stratification, through the Richardson number. This 3-D model has been designed to simulate meso-scale flows so that the modelling of the general circulation required adaptations of the turbulence closure to take into account the effect of meso-scale phenomena (Nihoul et al., 1989; Deleersnijder, 1992).

Arakawa's C-grid is used. The location of the dependent variables is in agreement with the staggering scheme of Blumberg and Mellor (1987), except that the turbulent kinetic energy is computed at the same point as temperature and salinity. The space discretisation follows the guide lines of the finite volume technique (Peyret and Taylor, 1983). Time derivatives are approximated by forward differences. All terms are calculated explicitly, with the noticeable exception of vertical turbulent fluxes, which are taken implicitly. The external mode is advanced in time according to the well-known forward–backward scheme (Mesinger and Arakawa, 1976). To represent the sea surface/bottom topography, use is made of the sigma coordinate system (Phillips, 1957; Freeman et al., 1972; Owen, 1980). Horizontal diffusion is introduced mostly "to damp small-scale computational noise" (Blumberg and Mellor, 1987) and is parameterized according to the recommendations of Mellor and Blumberg (1985).

As can be seen in Fig. 1, ISHTAR's domain of interest is delimited by long open sea boundaries. Part of the southern boundary crosses the Anadyr Strait, in which very interesting processes develop. In order to minimize the impact of open boundary conditions on the flow in the domain of interest, it was decided to set up a computational domain having boundaries sufficiently far away from the Anadyr Strait. The horizontal grid size was 10 km and each water column was divided into 10 grid boxes.

At the inflow boundary, the normal component of the transport was prescribed, by a process of trial and error, in such a way that two thirds of the northward flow passed through Anadyr Strait. The depth-dependency of the normal component of the horizontal velocity was simply assumed to be logarithmic. This too simple condition was the main cause of the spurious vertical motions taking place close to the inflow boundary, as will be seen below.

The initial temperature field was horizontally homogeneous with a marked thermocline at 15 m beneath the sea surface. No vertical dependence of the initial salinity field was prescribed. However, a horizontal salinity gradient was imposed in accordance with the water masses identified by Coachman et al. (1975). At the inflow boundary, the temperature and salinity profiles were held constant.

At the sea bed, the flux of temperature and salinity was prescribed to be zero. A slip boundary condition was used for the horizontal velocity. The drag coefficient was computed in accordance with the logarithmic layer theory (Blumberg and Mellor, 1987; Baumert and Radach, 1992; Davies and Gerritsen, 1993) and the roughness length was equal to 10^{-3} m.

At the outflow boundary, zero gradient conditions were used, except for the normal component of the transport which was imposed.

Table 1. *Analysis of monthly-averaged wind stress indicating whether or not wind-induced coastal upwelling is likely to exist in the vicinity of Anadyr Strait, according to the classical theory (Casanady, 1982)*

Month	Wind-induced Anadyr upwelling?
June 1984	no
July 1984	yes
August 1984	yes/no
September 1984	no
June 1985	no
July 1985	yes/no
August 1985	no
September 1985	no
June 1986	no
July 1986	yes
August 1986	no
September 1986	no

The wind data were kindly provided by C. Pease of NOAA/PMEL and were treated at Liège University by A. Mouchet.

No wind stress was applied in the boundary conditions of the momentum equations. Three reasons led to that choice.

First, as in one of the simulations of Overland and Roach (1987), the intent was to model the background flow, i.e., the circulation free of wind-induced variability.

Second, it was believed that the wind stress is not a major forcing of the flow in the domain of interest although, over the whole Bering/Ckukchi shelf, the wind stress has a major effect (Coachman et al., 1975; Aagaard et al., 1985; Spaulding et al., 1987). Indeed, model studies, briefly reported in Deleersnijder (1992), showed that the monthly wind stress is significantly smaller than the bottom stress in the domain of interest. This is obviously not the case everywhere in the Bering/Chukchi shelf because the vicinity of the Bering Strait is the shallowest part of the shelf. In fact, for a given flow, it is in the area where the sea depth is minimum that the velocity is likely to be maximum, so that it is precisely there that the bottom stress dominates the wind stress. If this reasoning turns out to be correct, it is clear that the wind forcing can be a determining factor in the general circulation on the Bering/Chukchi shelf while being of negligible importance locally, in the neighbourhood of the Bering Strait.

Third, the plume of cold water downstream of Anadyr Strait, although originating near the Siberian coast, does not seem to be caused by wind-induced coastal upwelling. Wind data indicate that the wind stress is hardly ever directed so as to drive coastal upwelling (Table 1). In other words, the Anadyr plume of cold water may well be due to an upwelling, but the driving force of that phenomenon is clearly not the wind stress. It was thus desirable to look for an upwelling mechanism in which the wind stress has no major role.

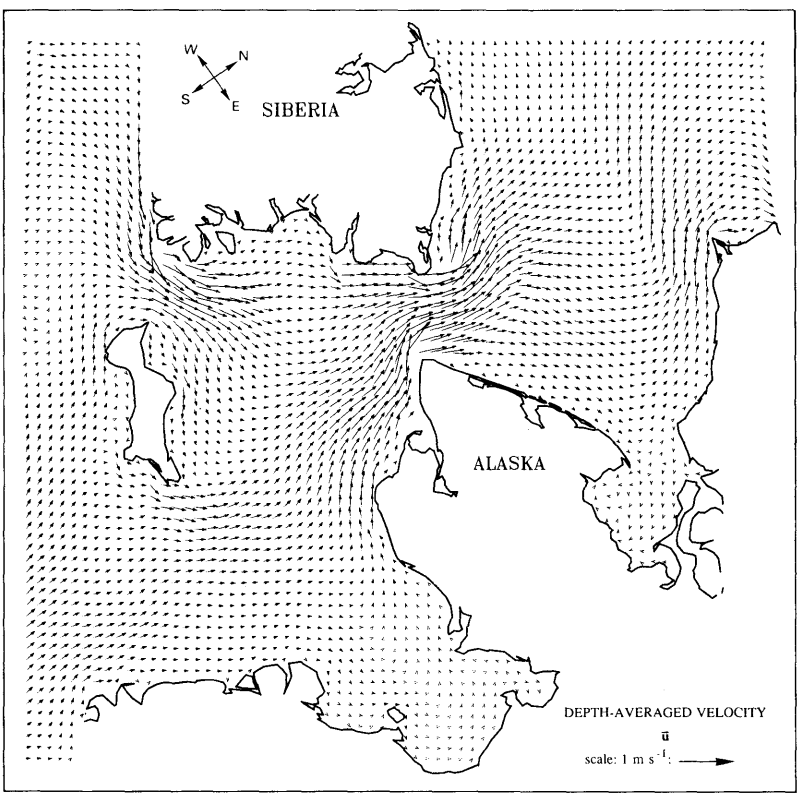

Fig. 4. Depth-averaged velocity field computed by the 3-D model.

Although no wind forcing was considered in the momentum balance, it was found appropriate to provide for some turbulence generation above the pycnocline. To do so, the turbulent kinetic energy at the sea surface was prescribed to be $2.8 \times 10^{-4}\ m^2\ s^{-2}$, which would correspond to a wind velocity of about $8\ m\ s^{-1}$. Furthermore, the Prandtl frequency, $|\partial \boldsymbol{u}/\partial z|$, used in the turbulent energy equation was constrained to be greater than a lower limit, established after a trial and error process. This limit was $N^2 \exp(-N^2/N_0^2)$, N being the Brunt-Vaisala frequency and $N_0^2 = 2 \times 10^{-4}\ s^{-2}$. This procedure, yet highly empirical, guaranteed a seemingly appropriate level of turbulent mixing above the pycnocline, producing temperature and salinity fields exhibiting small vertical variations near the surface, which was in agreement with the ISHTAR in situ observations.

As stated above, we are going to re-examine, with a particular focus on the vertical velocity, the model results described in Deleersnijder and Nihoul (1988a, 1988b), Deleersnijder (1989), Nihoul et al. (1989), Walsh et al. (1989b), Deleersnijder (1992), and Nihoul et al. (1993). In this simulation, the northward flow was set to 1.8 Sv, in agreement with early estimates of Coachman et al. (1975). In the light of more recent studies, this flow is probably too high (Coachman and Aagaard, 1988; Walsh et al., 1989b). However, other numerical results, briefly reported in Deleersnijder (1992), have shown that, when the northward flow is between 0.8 and 2 Sv, the three components of the velocity approximately scale with the value of the global flow. It thus seems legitimate to concentrate the present analysis on the results of GHER's model that have been most extensively examined so far.

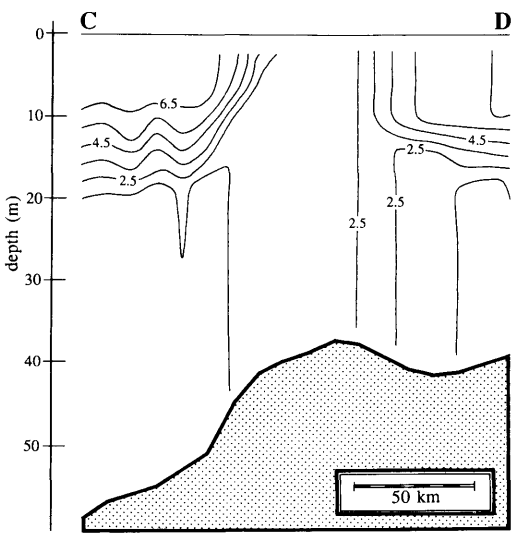

Fig. 5. Modelled temperature (°C) in the plane of section CD. The location of the plane of section is indicated in Fig. 1.

The model ran until the velocity field attained a steady state, of which the depth-averaged horizontal velocity is displayed in Fig. 4. This velocity field proved to be in good agreement with the measurements of Tripp (1985, 1986) in the Anadyr Strait, in the Chirikov Basin and in the Bering Strait (Deleersnijder, 1992; Nihoul et al., 1993). In view of other models' results (Liu and Leenderste, 1987; Overland and Roach, 1987; Spaulding et al., 1987; Brasseur, 1991) and of the general circulation scheme of Takenouti and Ohtani (1974), it seems that the direction of the velocity south of St-Lawrence Island is wrong. Nevertheless, in the absence of current data from this region, it is hard to make a final decision on this particular point.

Examining Figs. 1, 4, one sees that the flow roughly follows the isobaths, which is due to the fact the horizontal velocity is nearly in geostrophic equilibrium with the pressure forces related to the variations of the sea surface elevation.

The computed temperature field reflects the presence of strong vertical fluxes in the Anadyr Strait (Fig. 5), which is qualitatively in agreement with all of the temperature data referred to above.

3. The vertical velocity

As previously mentioned, the equations of the model are solved numerically in the sigma-coordinate system, which means that the physical space-time coordinates (t, x_1, x_2, x_3) are transformed to new coordinates as follows:

$$(\tilde{t}, \tilde{x}_1, \tilde{x}_2, \tilde{x}_3) = \left(t, x_1, x_2, L\frac{x_3 + h}{\eta + h} = L\sigma \right), \qquad (1)$$

where t denotes time; x_1 and x_2 are the horizontal coordinates; x_3 represents the vertical coordinate in such a way that the sea surface is located at $x_3 = \eta$ and the sea bottom at $x_3 = -h$, with

$h(x_1, x_2) \geqslant 0$. In the sigma-space, the depth of the computational domain, L, is constant.

Along with (1), it is customary to introduce a new vertical velocity, $\tilde{u}_3$, defined as the material derivative of $\tilde{x}_3$, i.e.,

$$\tilde{u}_3 = \frac{\partial \tilde{x}_3}{\partial t} + \boldsymbol{u} \cdot \nabla \tilde{x}_3 + u_3 \frac{\partial \tilde{x}_3}{\partial x_3}, \tag{2}$$

where $\boldsymbol{u}$ and u_3 denote the horizontal velocity vector and the vertical velocity (positive upwards), respectively; ∇ is the horizontal "gradient operator",

$$\nabla = \boldsymbol{e}_1 \frac{\partial}{\partial x_1} + \boldsymbol{e}_2 \frac{\partial}{\partial x_2}. \tag{3}$$

Unit vectors $\boldsymbol{e}_1$ and $\boldsymbol{e}_2$ are horizontal and are associated with coordinates x_1 and x_2, respectively.

Using $\tilde{u}_3$ has two distinct advantages. First, in the sigma-coordinate system, the equations of marine models have a much simpler form if $\tilde{u}_3$ is used instead of u_3. Second, taking into account the impermeability of the bottom ($\sigma = 0$) and the surface ($\sigma = 1$) turns out to be very easy because the impermeability conditions simply read:

$$[\tilde{u}_3]_{\sigma = 0,1} = 0. \tag{4}$$

The computation of u_3 is part of the postprocessing of the results of the model. From a numerical point of view, this task is better achieved by using the conservative formula suggested by Deleersnijder (1989) than by simply inverting definition (2).

Waleffe (1985) first suggested that it could be appropriate to identify the "geometrical" part of the vertical velocity. This idea, later extended by Deleersnijder (1989), led to the splitting of u_3 into two components, namely the upsloping velocity, w_{US}, Waleffe's (1985) "geometrical" velocity, and the upwelling velocity, w_{UW}. Accordingly, one may write:

$$u_3 = w_{US} + w_{UW}. \tag{5}$$

For time-independent flows, w_{US} and w_{UW} read

$$w_{US} = -\boldsymbol{u} \cdot [(1-\sigma)\nabla h - \sigma \nabla \eta] \tag{6}$$

and

$$w_{UW} = \frac{H}{L} \tilde{u}_3, \tag{7}$$

with $H = h + \eta$ representing the total height of the water column.

Let the vertical unit vector be defined by $\boldsymbol{e}_3 = \boldsymbol{e}_1 \times \boldsymbol{e}_2$. It may be seen that a particle moving with a velocity equal to $\boldsymbol{u} + w_{US}\boldsymbol{e}_3$ does not cross any iso-σ surface, which means that this particle remains at the same relative height in the water column. Since the bottom and the surface are iso-σ surfaces, w_{US} may be interpreted as the vertical adapted to the slope of the surface and the bottom.

The upwelling velocity w_{UW} is the velocity with which the water crosses the iso-σ surfaces. As a consequence, w_{UW} may be viewed as the vertical velocity associated with the true up- and downwelling motions.

Decomposition (5) provides one with a useful interpretation tool (Deleersnijder et al., 1992), since it renders it possible to distinguish between the part of the vertical velocity that is necessary for the flow to accomodate to the geometry of the basin and the extra vertical velocity related to actual up- or down-wellings.

A significant drawback must nevertheless be highlighted. Eqs. (6) and (7) are purely arbitrary: it is indeed possible to put forward several definitions of w_{US} and w_{UW} that could be equally valid as regards the distinction between the motions that are associated with the geometry of the basin and those that are not. What justifies (6) and (7) is only that they take advantage in a very natural way of the use of the sigma-coordinate system. In a certain sense, (6) and (7) are inherent in the sigma-transformation.

In accordance with the above reasoning, we will examine the upsloping and upwelling velocities separately.

4. Analysis of the upsloping velocity

To understand the space distribution of the upsloping velocity, it is desirable to identify the dominant terms of definition (6). The sea surface elevation does not exceed ± 0.4 m (Deleersnijder and Nihoul, 1988b). Hence, in (5), $\sigma \nabla \eta$ may be neglected compared with $(1-\sigma)\nabla h$. Let $\hat{\boldsymbol{u}} \equiv \boldsymbol{u} - \bar{\boldsymbol{u}}$

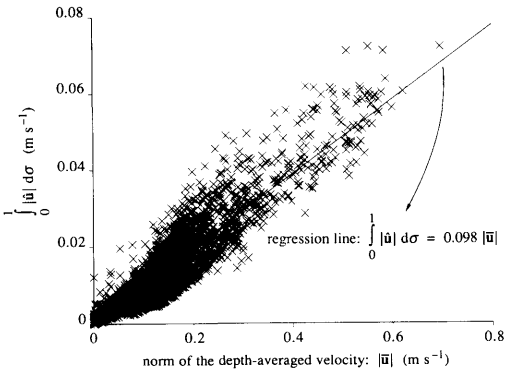

Fig. 6. Scatter plot of the depth-average of $|\hat{u}|$ as a function of $|\bar{u}|$ constructed with all water columns of the model.

denote the deviation of the horizontal velocity relative to its depth-averaged value

$$\bar{u} = \int_0^1 u \, d\sigma. \tag{8}$$

In Fig. 6, one immediately sees that $|\hat{u}|$ is, in general, much smaller than $|\bar{u}|$. It is thus suggested to approximate w_{US} by a "simplified upsloping velocity" defined as

$$w_{US,S} = -(1-\sigma)\,\bar{u}\cdot\nabla H. \tag{9}$$

In a grid box adjacent to a lateral solid boundary, the numerical evaluation of (9) may be delicate. By combining (9) with the depth-integrated continuity equation for steady flows,

$$\nabla\cdot(H\bar{u}) = 0, \tag{10}$$

one readily obtains

$$w_{US,S} = (1-\sigma)\,H\nabla\cdot\bar{u}. \tag{11}$$

From a numerical point of view, the latter expression is more appropriate than (9), since it permits taking into account in a proper way that the component of $\bar{u}$ normal to a solid boundary is zero.

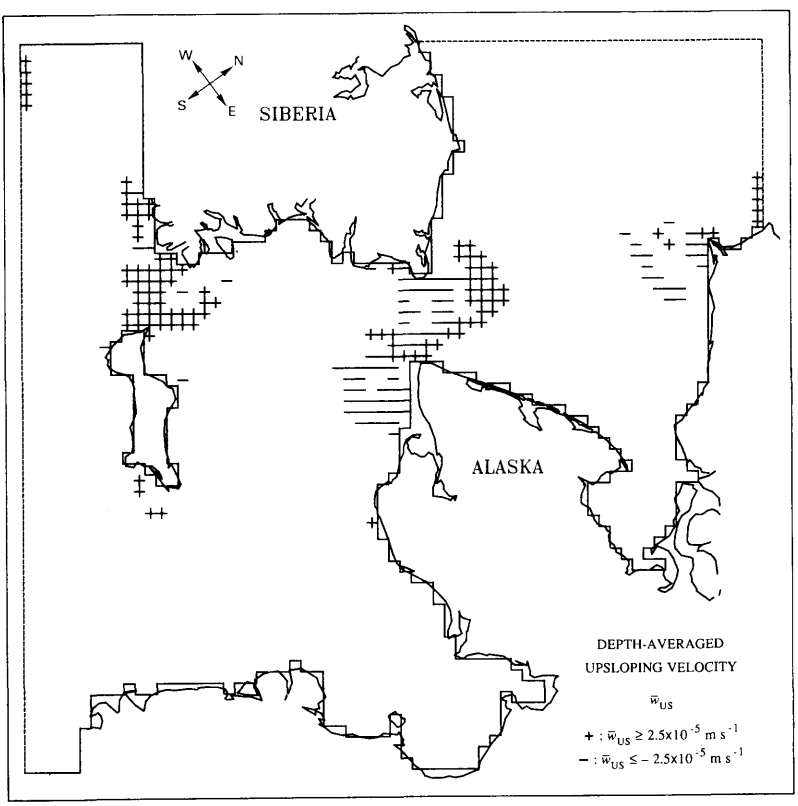

Fig. 7. Depth-averaged upsloping velocity.

The simplified upsloping velocity turns out to be reasonably close to w_{US}. Indeed, upon denoting $|s|_{rms}$ the root mean square taken over the whole computational domain of a function s, the analysis of the w_{US} and $w_{US,S}$ fields yields

$$\frac{|w_{US,S} - w_{US}|_{rms}}{|w_{US}|_{rms}} = 0.24 \tag{12}$$

which means that $w_{US,S}$, roughly speaking, accounts for 76% of w_{US}.

The most advantageous feature of the simplified upsloping velocity is that, over each water column, the values of $w_{US,S}$ are self-similar: $|w_{US,S}/(H\nabla\cdot\bar{\boldsymbol{u}})|$ is a function of σ only, which is zero at the surface and maximum at the bottom.

Since w_{US} is close to $w_{US,S}$, the vertical profiles of the upsloping velocity are nearly self-similar. As a result, to interpret the 3-D field of w_{US}, it is sufficient to display a depth-independent quantity such as, for instance, the depth-mean upsloping velocity $\bar{w}_{US}$ (Fig. 7). It would be less appropriate to simply display the upsloping velocity in a series of horizontal planes of section located at various depths below the surface. Doing that would result in confusing pictures in which it would be difficult to distinguish between the horizontal variability of w_{US} that is intrinsic to the flow and that associated with the plane of section being, from one location to another, relatively closer or more distant to the sea surface or the sea bottom. In that respect, it is illuminating to examine expression (9) together with the definition of σ.

Looking simultaneously at Figs. 1, 4, and 7, one immediately notices that, as expected, the upsloping velocity is positive where the flow is directed towards shallower regions and is negative otherwise. Furthermore, in agreement with (9), $|\bar{w}_{US}|$ is maximum in the vicinity of Anadyr and Bering Straits, i.e., in the regions where the horizontal current most clearly crosses the isobaths while having a large speed. In particular, the upsloping velocity is high in the Anadyr Strait, indicating significant upwards water fluxes.

It must be pointed out that the upsloping velocity cannot bring a water parcel up to the surface. However, when the upsloping velocity is positive, every water parcel comes closer to the surface, while remaining at the same relative height in the water column. This may render it more likely for the turbulent diffusion to mix some of the water column, or even the whole water column, since the height of fluid to be mixed decreases. Whether or not this hypothesis is correct is difficult to verify, because this mechanism involves two processes interacting non-linearly. Anyway, this process, if it actually exists, could be responsible for part of the cold water plume developing downstream of the Anadyr Strait.

The vertical eddy coefficients are of order $10^{-1} - 10^{-2}\,m^2\,s^{-1}$ (Deleersnijder and Nihoul, 1988b; Deleersnijder, 1992). Thus, taking $10^{-4}\,m\,s^{-1}$ and 40 m as the vertical velocity scale and the vertical length scale, respectively, it is seen that the order of magnitude of the vertical turbulent Reynolds number is 0.4–0.04. Hence, one might think that the vertical turbulent fluxes markedly dominate the vertical advection. This is partly correct only, since in the region of the thermocline the vertical diffusivities decrease by several order of magnitude to their molecular values ($\approx 10^{-6} - 10^{-8}\,m^2\,s^{-1}$). However, away from the thermocline, the scalar quantities are well mixed by the turbulent diffusion. To summarize, the vertical turbulent diffusion clearly dominates the vertical advection, except in the region of the thermocline, where the vertical advection is likely to be much larger.

5. Analysis of the upwelling velocity

For a given water column, let the upwelling velocity be written as

$$w_{UW} = w_{UW,+} + w_{UW,-}, \tag{13a}$$

with

$$w_{UW,+} = \frac{\mathrm{sign}(\bar{w}_{UW}) + 1}{2} w_{UW}, \tag{13b}$$

$$w_{UW,-} = -\frac{\mathrm{sign}(\bar{w}_{UW}) - 1}{2} w_{UW}, \tag{13c}$$

where $\bar{w}_{UW}$ represents the depth-average of w_{UW}; "sign" is a function that is equal to $+1$ or -1 according to whether its argument is positive or negative. Analysis of the model results leads to:

$$\frac{|w_{UW,-}|_{rms}}{|w_{UW,+}|_{rms}} = 0.05, \tag{14}$$

which means that, along the vertical coordinate, changes of sign of the upwelling velocity are of negligible importance. In fact, most vertical profiles of w_{UW} are of the same type: as σ increases from 0 to 1, $|w_{UW}|$ grows from zero at the bottom, then reaches a maximum and finally decreases to zero at the surface. However, the location of the maximum of $|w_{UW}|$ may vary widely from one vertical to another.

Although the vertical profiles of w_{UW} are not close to being self-similar, they exhibit enough common features for a method resembling that used to display w_{US} to be utilized for the graphical representation of the field of upwelling velocity (Fig. 8).

Significant up- and down-welling motions are found in small areas (Fig. 8). Upwelling phenomena taking place in the one grid box wide strip along the southern open boundary clearly correspond to an artefact due to improper boundary conditions imposed on the horizontal velocity (Deleersnijder, 1992). In the region of the Anadyr Strait, close to the Siberian coast, the upwelling velocity is directed upwards and can be as high as 10 m day^{-1}. Thus, the upwelling velocity is large enough to bring the thermocline, initially located at $x_3 = -15$ m, up to the sea surface, as can be seen in Fig. 5, and in the modelled temperature fields displayed in Deleersnijder and Nihoul (1988a, b) and Deleersnijder (1992).

The vertical velocity in the sigma-space is computed from the continuity equation by the following expression

$$\tilde{u}_3 = -\frac{L}{H}\int_0^{\sigma} \tilde{\nabla} \cdot (H\hat{\boldsymbol{u}})\, \mathrm{d}\sigma, \tag{15}$$

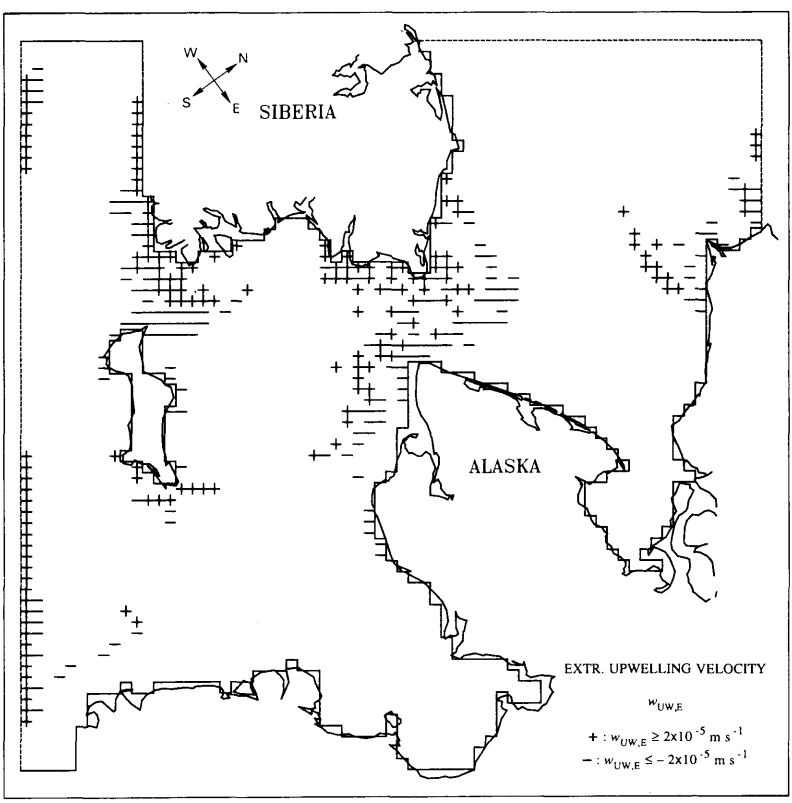

Fig. 8. Representation of the upwelling velocity. For each water column, one takes into account the extremum upwelling velocity $w_{UW,E}$, i.e., the value of w_{UW} that has the maximum absolute value.

with

$$\tilde{\nabla} = \boldsymbol{e}_1 \frac{\partial}{\partial \tilde{x}_1} + \boldsymbol{e}_2 \frac{\partial}{\partial \tilde{x}_2}. \tag{16}$$

Vertical velocity $\tilde{u}_3$ is proportional to L, but it is readily understood that the other dependent variables of the model, horizontal velocity, temperature, do not depend upon L. If the value of L is chosen to be of the same order of magnitude as the horizontal length scale, then the computational domain is isotropic in the sigma-space. Hence, if upwelling motions are important, $|\tilde{u}_3|$ will be comparable to $|\boldsymbol{u}|$. This is not the case, since, with $L = 10^5$ m, one has

$$\frac{|\tilde{\boldsymbol{u}}_3|_{\text{rms}}}{\|\boldsymbol{u}\|_{\text{rms}}} = 0.17. \tag{17}$$

This result is in accordance with a simple scaling of relation (15) in which the smallness of $|\hat{\boldsymbol{u}}|$ relative to $|\boldsymbol{u}|$ is taken into account.

The smallness of ratio (17) means that the up- and down-wellings are overall not very important. It is nevertheless in agreement with the fact that it is only in small areas, where the variability of $H\hat{\boldsymbol{u}}$ is high, that the vertical advection may be significant, as illustrated in Fig. 8.

6. Mechanism of the up- and down-wellings

As previously explained, the wind forcing is not the main cause of the vertical motions. It follows that one has to look for another upwelling mechanism. Inspiration can be found in the Ekman pumping theory set out in classical treatises of geophysical fluid dynamics (Pedlosky, 1979; Gill, 1982).

From eq. (15), it follows that one has to analyse the behaviour of $H\hat{\boldsymbol{u}}$ in order to understand the distribution of $\tilde{u}_3$ and, hence, of w_{UW}.

The direction of $\boldsymbol{u}$ with respect to $\bar{\boldsymbol{u}}$ is measured by the angle ξ, which may be calculated from:

$$\sin \xi = \frac{\boldsymbol{e}_3 \cdot (\bar{\boldsymbol{u}} \times \boldsymbol{u})}{|\boldsymbol{u}|\,|\bar{\boldsymbol{u}}|}. \tag{18}$$

Angle ξ is positive if $\boldsymbol{u}$ is "on the left of $\bar{\boldsymbol{u}}$", and is negative otherwise. For each water column, the veering Ξ is defined as

$$\Xi = \xi_{\max} - \xi_{\min}, \tag{19a}$$

if the point where $\xi = \xi_{\max}$ is closer to the bottom than that where $\xi = \xi_{\min}$. Otherwise,

$$\Xi = -(\xi_{\max} - \xi_{\min}). \tag{19b}$$

The veering is positive in 2556 verticals out of a total of 2690. In other words, in 95% of the verticals of the computational domain, the direction of $\boldsymbol{u}$ is qualitatively in accordance with that of the bottom Ekman spiral, i.e., $\boldsymbol{u}$ is on the left of $\bar{\boldsymbol{u}}$ near the bottom and on the right of $\bar{\boldsymbol{u}}$ near the surface (Fig. 9). This is not surprising, since it may be shown that the Ekman momentum equation,

$$f\boldsymbol{e}_3 \times \boldsymbol{u} \sim -g\nabla\eta + \frac{\partial}{\partial x_3}\left(\nu_{\text{T}} \frac{\partial \boldsymbol{u}}{\partial x_3}\right), \tag{20}$$

encompasses the dominant terms of the horizontal momentum equations (Deleersnijder, 1992). In (20), f, g, and ν_{T} represent the Coriolis factor ($\approx 1.3 \times 10^{-4}\ \text{s}^{-1}$), the gravitational acceleration, and the vertical eddy viscosity, respectively. In other words, advection and horizontal diffusion of

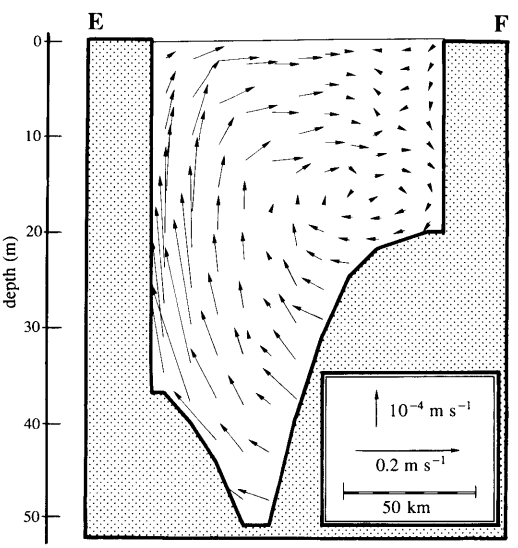

Fig. 9. Velocity $\hat{u}_2\boldsymbol{e}_2 + u_3\boldsymbol{e}_3$ in the plane of section EF, the position of which is indicated in Fig. 1. Notice that horizontal unit vector $\boldsymbol{e}_2$ is parallel to EF.

momentum as well as the baroclinic pressure gradient are small throughout much of the domain, as could be expected from order of magnitude analysis.

The validity of approximation (20) may be illustrated in a simple way by examining its depth-average,

$$f\boldsymbol{e}_3 \times \bar{\boldsymbol{u}} \sim -g\nabla\eta - \frac{\tau^b}{H}, \tag{21}$$

where τ^b is the bottom stress divided by the water density. From (21), a horizontal velocity $\boldsymbol{u}_e$, which we propose to call "Ekman velocity", may be derived:

$$f\boldsymbol{e}_3 \times \boldsymbol{u}_e = -g\nabla\eta - \frac{\tau^b}{H}, \tag{22}$$

so that

$$\boldsymbol{u}_e = \frac{g}{f}\boldsymbol{e}_3 \times \nabla\eta + \frac{1}{fH}\boldsymbol{e}_3 \times \tau^b. \tag{23}$$

After some manipulations of the model results, one obtains

$$\frac{\|\boldsymbol{u}_e - \bar{\boldsymbol{u}}\|_{rms}}{\|\bar{\boldsymbol{u}}\|_{rms}} = 0.09, \tag{24}$$

which means that $\boldsymbol{u}_e$ is an excellent approximation of $\bar{\boldsymbol{u}}$ (Fig. 10).

The qualitative properties of $H\hat{\boldsymbol{u}}$ are accounted for in the following Taylor expansions of $H\hat{\boldsymbol{u}}$ truncated at two terms:

$$H\hat{\boldsymbol{u}} = (H\hat{\boldsymbol{u}})_{\parallel} + (H\hat{\boldsymbol{u}})_{\perp}, \tag{25}$$

with

$$(H\hat{\boldsymbol{u}})_{\parallel} = -a_{\parallel}(1-2\sigma)\, H\bar{\boldsymbol{u}}, \tag{26a}$$

$$(H\hat{\boldsymbol{u}})_{\perp} = a_{\perp}(1-2\sigma)\, \boldsymbol{e}_3 \times H\bar{\boldsymbol{u}}, \tag{26b}$$

where $a_{\parallel}$ and $a_{\perp}$ are positive constants. Relations (25) and (26) are by no means intended to provide a reliable approximation to the vertical profiles of $H\hat{\boldsymbol{u}}$. Instead, (25)–(26) are simply caricatured formulae having some of the modelled properties of $H\hat{\boldsymbol{u}}$: in (25)–(26), the depth-average of $|\hat{\boldsymbol{u}}|$ is a linearly increasing function of $|\bar{\boldsymbol{u}}|$, and the veering is always positive. Combining (7), (15), (25), and (26), one gets

$$w_{UW} = a_{\perp}\boldsymbol{e}_3 \cdot (\nabla \times H\bar{\boldsymbol{u}})\, \sigma(1-\sigma), \tag{27}$$

which implies

$$\text{sign}(\bar{w}_{UW}) = \text{sign}[\boldsymbol{e}_3 \cdot (\nabla \times H\bar{\boldsymbol{u}})]. \tag{28}$$

Whether or not the sign of the upwelling velocity is actually given by the sign of the curl of the transport is easily checked. It turns out that (28) provides an excellent account of the model results (Table 2).

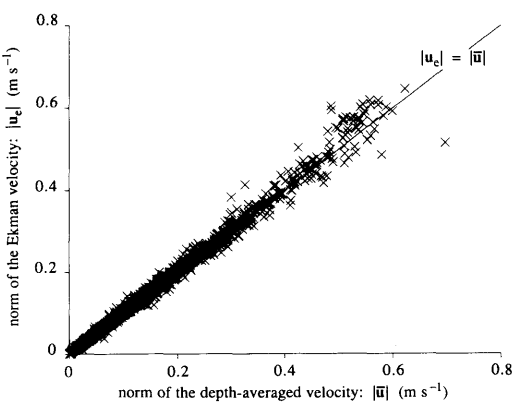

Fig. 10. Scatter plot of $|\boldsymbol{u}_e|$ as a function of $|\bar{\boldsymbol{u}}|$ constructed with all water columns of the model.

Table 2. *Verification of eq. (28)*

$\lvert\bar{w}_{UW}\rvert$ (10^{-5} m s^{-1})	n_+	n_-	$\frac{n_+}{n_+ + n_-}$
≥ 0.1	1547	315	0.83
≥ 0.5	531	126	0.81
≥ 1	240	69	0.78
≥ 2	78	13	0.86
≥ 3	30	3	0.91
≥ 4	17	1	0.94
≥ 5	10	1	0.91
≥ 6	5	0	1.0
≥ 7	1	0	1.0
≥ 8	0	0	—

n_+ denotes the number of water columns where the sign of the depth-averaged upwelling velocity is equal to that of $\boldsymbol{e}_3 \cdot (\nabla \times H\bar{\boldsymbol{u}})$ and n_- denotes the number of water columns where (28) does not apply.

The mechanism of the up- and down-wellings is thus as follows. The main driving force of the horizontal velocity is the part of the pressure gradient that is associated with the variations of the sea surface elevation. Due to the frictional forces associated with the bottom stress, the horizontal velocity is not identically equal to its depth-mean. Moreover, the Coriolis force induces a positive veering of the velocity. The resulting space variations of $(H\hat{\boldsymbol{u}})_{\perp}$, correlated with those of $H\bar{\boldsymbol{u}}$, lead to local divergence or convergence of $H\hat{\boldsymbol{u}}$, implying vertical motion in the sigma-space. The variations of $(H\hat{\boldsymbol{u}})_{\parallel}$ have no impact on w_{UW}, which is reasonably well confirmed by the model results (Deleersnijder, 1992).

What has been done above simply amounts to adapting the Ekman pumping theory to our results, where the bottom stress turns out to be the ultimate cause of the vertical motions. No claim is made that (28) could be applied to the results of other 3-D hydrodynamical studies.

Formula (28) implies that there should be coastal upwelling when the current is such that the water moves "with the land on its left". Indeed, if $\boldsymbol{t}$ denotes the unit vector tangential to the coastline, one may approximate $H\bar{\boldsymbol{u}}$ in the vicinity of the coastline by

$$H\bar{\boldsymbol{u}} \sim U_t \boldsymbol{t}, \tag{29}$$

with $U_t > 0$. Introducing (29) into (28), assuming that the variations of U_t are predominantly in the direction normal to the coastline, one obtains

$$\boldsymbol{e}_3 \cdot (\nabla \times H\bar{\boldsymbol{u}}) \sim \frac{\partial U_t}{\partial n} > 0 \Rightarrow \bar{w}_{\mathrm{UW}} > 0, \tag{30}$$

with

$$\frac{\partial}{\partial n} = \boldsymbol{n} \cdot \nabla, \tag{31}$$

where $\boldsymbol{n} = -\boldsymbol{e}_3 \times \boldsymbol{t}$ is the unit vector normal to the coastline. Conversely, if the water flows "with the land on its right" ($U_t < 0$), the same kind of reasoning suggests downwelling taking place near the coast. The above development seems to be in agreement with the model results, since there is mostly upwelling near the Siberian coast and downwelling near the Alaskan (Fig. 8).

7. Conclusion

The vertical velocity field, produced by the GHER 3-D model, has been analysed by a method requiring the splitting of the real vertical velocity into two components, namely the upsloping velocity and the upwelling velocity. This technique has been shown to work rather well for two main reasons. First, the upsloping and upwelling velocities are associated with different processes. Second, their typical vertical profiles are completely different.

The vertical velocity field produced by the model in the vicinity of Anadyr Strait is qualitatively in agreement with the observations. According to the results of the model, the Anadyr Strait plume of cold water is due to an upwelling process, possibly combined with upsloping and turbulent diffusion.

The upwelling mechanism found in the simulated currents closely resembles the classical Ekman pumping process, which is a concept generally used in deep seas. It is proposed to introduce the notion of shallow sea Ekman pumping, a mechanism that concerns the whole water column.

8. Acknowledgements

The advice of ISHTAR participants is acknowledged. ISHTAR was supported by the US National Science Foundation. The author is indebted to Professor Nihoul for his guidance during the design and the use of the three-dimensional model applied to the region of the Bering Strait. Part of the work presented here has been done when the author was Research Assistant at the National Fund for Scientific Research of Belgium. André Joris was of great help in the preparation of some of the figures. Kevin Ruddick is acknowledged for reviewing the first version of this article. An anonymous referee provided several thoughtful comments on the manuscript.

REFERENCES

Aagaard, K., Roach, A. T. and Schumacher, J. D. 1985. On the wind-driven variability of the flow through the Bering Strait. *J. Geophys. Res.* **90**, 7213–7221.

Baumert, H. and Radach, G. 1992. Hysteresis of turbulent kinetic energy in nonrotational tidal flows: a model study. *J. Geophys. Res.* **97**, 3669–3677.

Beckers, J.-M. 1991. Application of the GHER 3D general circulation model to the Western Mediterranean. *J. Mar. Syst.* **1**, 315–332.

Blumberg, A. F. and Mellor, G. L. A description of a three-dimensional coastal ocean circulation model. In: *Three-dimensional coastal ocean models* (ed. N. S. Heaps). American Geophysical Union, Washington, DC, 1–16.

Brasseur, P. P. 1991. A variational inverse method for the reconstruction of general circulation fields in the Northern Bering Sea. *J. Geophys. Res.* **96**, 4891–4907.

Brasseur, P. P. and Haus, J. A. 1991. Application of a 3-D variational inverse model to the analysis of ecohydrodynamic data in the Northern Bering and Southern Chukchi Seas. *J. Mar. Syst.* **1**, 383–401.

Coachman, L. K. 1986. Circulation, water masses, and fluxes on the Southeastern Bering Shelf. *Cont. Shelf Res.* **5**, 23–108.

Coachman, L. K. and Aagaard, K. 1966. On the water exchange through Bering Strait. *Limnol. Oceanogr.* **11**, 44–59.

Coachman, L. K. and Aagaard, K. 1988. Transports through Bering Strait: annual and interannual variability. *J. Geophys. Res.* **93**, 15535–15539.

Coachman, L. K., Aagaard, K. and Tripp, R. B. 1975. *Bering Strait: the regional physical oceanography.* University of Washington Press, Seattle, 172 pp.

Coachman, L. K. and Shigaev, V. V. 1992. Northern Bering–Chukchi Sea ecosystem: the physical basis. In: *Results of the third joint US-USSR Bering and Chukchi seas expedition (BERPAC), summer 1988* (ed. P. A. Nagel). U.S. Fish and Wildlife Service, Washington, DC, 17–27.

Csanady, G. T. 1982. *Circulation in the coastal ocean.* D. Reidel, Dordrecht, 279 pp.

Davies, A. M. and Gerritsen, H. 1993. An intercomparison of three-dimensional tidal hydrodynamic models of the Irish Sea. *Tellus*, in press.

Deleersnijder, E. 1989. Upwelling and upsloping in three-dimensional marine models. *Appl. Math. Model.* **13**, 462–467.

Deleersnijder, E. 1992. *Modélisation hydrodynamique tridimensionnelle de la circulation générale estivale de la région du Détroit de Bering.* Thèse de Doctorat, Faculté des Sciences Appliquées, Université Catholique de Louvain, 189 pp.

Deleersnijder, E. and Nihoul, J. C. J. 1988a. Turbulent fields associated with the general circulation in the Northern Bering Sea. In: *Small-scale turbulence and mixing* (eds. J. C. J. Nihoul and B. M. Jamart). Elsevier, Amsterdam, 77–94.

Deleersnijder, E. and Nihoul, J. C. J. 1988b. General circulation in the Northern Bering Sea. ISHTAR Annual Progress Report, University of Liège, 392 pp.

Deleersnijder, E., Norro, A. and Wolanski, E. 1992. A three-dimensional model of the water circulation around an island in shallow water. *Cont. Shelf Res.* **12**, 891–906.

Freeman, N. G., Hale, A. M. and Danard, M. B. 1972. A modified sigma equations' approach to the numerical modeling of Great Lakes hydrodynamics. *J. Geophys. Res.* **77**, 1050–1060.

Gill, A. E. 1982. *Atmosphere-ocean dynamics.* Academic Press, San Diego, 662 pp.

Haus, J. 1991. Variational inverse modelling, Data analyses via reconstruction of 3-D fields. Mémoire de D.E.A. an modélisation de l'environnement marin, Programme Erasmus, Université de Liège, 88 pp.

Kinder, T. H., Chapman, D. C. and Whitehead, J. A., Jr. 1986. Westward intensification of the mean circulation on the Bering Sea shelf. *J. Phys. Oceanogr.* **16**, 1217–1229.

Liu, S. K. and Leendertse, J. J. 1987. Modeling the Alaskan continental shelf waters. The RAND Corporation (R/3567-NOAA/RC), Santa Monica, California, 136 pp.

Mellor, G. L. and Blumberg, A. F. 1985. Modeling vertical and horizontal diffusivities with sigma coordinate system. *Mon. Weather Rev.* **113**, 1379–1383.

Mellor, G. L. and Yamada, T. 1982. Development of a turbulence closure model for geophysical fluid problems. *Rev. Geophys. Space Phys.* **20**, 851–875.

Mesinger, F. and Arakawa, A. 1976. Numerical methods used in atmospheric models. In: *GARP Publications Series* (no. 17, vol. 1). WM0-ICSU Joint Organizing Committee, 64 pp.

Mofjeld, H. O. 1986. Observed tides on the Northeastern Bering shelf. *J. Geophys. Res.* **91**, 2593–2606.

Nihoul, J. C. J. 1984. A three-dimensional general marine circulation model in a remote sensing perspective. *Ann. Geophys.* **2**, 433–442.

Nihoul, J. C. J. 1986. Aspects of the Northern Bering Sea ecohydrodynamics. In: *Marine interfaces ecohydrodynamics* (ed. J. C. J. Nihoul). Elsevier, Amsterdam, 385–399.

Nihoul, J. C. J., Adam, P., Brasseur, P., Deleersnijder, E. and Djenidi, S. 1993. Three-dimensional general circulation model of the Northern Bering Sea's summer ecohydrodynamics. *Cont. Shelf Res.* **13**, 509–542.

Nihoul, J. C. J., Deleersnijder, E. and Djenidi, S. 1989. Modelling the general circulation of shelf seas by 3D $k-\varepsilon$ models. *Earth-Sci. Rev.* **26**, 163–189.

Nihoul, J. C. J. and Djenidi, S. 1987. Perspective in three-dimensional modelling of the marine systems. In: *Three-dimensional models of marine and estuarine dynamics* (eds. J. C. J. Nihoul and B. M. Jamart). Elsevier, Amsterdam, 1–33.

Nihoul, J. C. J., Waleffe, F. and Djenidi, S. 1986. A 3D-numerical model of the Northern Bering Sea. *Environ. Softw.* **1**, 76–81.

Overland, J. E. and Roach, A. T. 1987. Northward flow in the Bering and Chukchi Seas. *J. Geophys. Res.* **92**, 7097–7105.

Owen, A. 1980. A three-dimensional model of the Bristol Channel. *J. Phys. Oceanogr.* **10**, 1290–1302.

Pedlosky, J. 1979. *Geophysical fluid dynamics.* Springer-Verlag, New York, 624 pp.

Peyret, R. and Taylor, T. D. 1983. *Computational*

Tellus A/46/2-4*

methods for fluid flow. Springer-Verlag, New York, 358 pp.

Phillips, N. A. 1957. A coordinate system having some special advantages for numerical forecasting. *J. Meteorol.* **14**, 184–185.

Rodi, W. 1987. Examples of calculation methods for flow and mixing in stratified fluids. *J. Geophys. Res.* **92**, 5305–5328.

Sambrotto, R. N., Goering, J. J. and McRoy, C. P. 1984. Large yearly production of phytoplankton in the Western Bering Strait. *Science* **225**, 1147–1149.

Spaulding, M., Isaji, T., Mendelsohn, D. and Turner, A. C. 1987. Numerical simulation of wind-driven flow through the Bering Strait. *J. Phys. Oceanogr.* **17**, 1799–1816.

Stigebrandt, A. 1984. The North Pacific: a global scale estuary. *J. Phys. Oceanogr.* **14**, 464–470.

Takenouti, A. Y. and Ohtani, K. 1974. Currents and water masses in the Bering Sea: a review of Japanese work. In: *Oceanography of the Bering Sea* (eds. D. W. Hood and E. J. Kelley). Institute of Marine Science, University of Alaska, Fairbanks, USA, 39–57.

Tripp, R. B. 1985. *1985 current meter and pressure gauge data*. ISHTAR Data Report, University of Alaska, Fairbanks.

Tripp, R. B. 1986. *1986 current meter and pressure gauge data*. ISHTAR Data Report, University of Alaska, Fairbanks.

Waleffe, F. 1985. *Modèle mathématique 3D de la Mer de Bering*. Mémoire de fin d'études, Faculté des Sciences Appliquées, Université de Liège, 126 pp.

Walsh, J. J. and Dieterle, D. A. 1986. Simulation analysis of plankton dynamics in the Northern Bering Sea. In: *Marine interfaces ecohydrodynamics* (ed. J. C. J. Nihoul). Elsevier, Amsterdam, 401–428.

Walsh, J. J., McRoy, C. P., Blackburn, T. H., Coachman, L. K., Goering, J. J., Henriksen, K., Andersen, P., Nihoul, J. C. J., Parker, P. L., Springer, A. M., Tripp, R. B., Whitledge, T. E. and Wirick, C. D. 1989a. The role of the Bering Strait in the carbon/nitrogen fluxes of polar marine ecosystems. In: *Proceedings of the 6th Conference of the Comité Arctique International* (eds. L. Rey and V. Alexander). E. J. Brill, Leiden, 90–120.

Walsh, J. J., McRoy, C. P., Coachman, L. K., Goering, J. J., Nihoul, J. C. P., Whitledge, T. E., Blackburn, T. H., Parker, P. L., Wirick, C. D., Shuert, P. G., Grebmeier, J. M., Springer, A. M., Tripp, R. B., Hansell, D. A., Djenidi, S., Deleersnijder, E., Henriksen, K., Lund, B. A., Andersen, P., Müller-Karger, F. E. and Dean, K. 1989b. Carbon and nitrogen cycling within the Bering/Chukchi Seas: source regions for organic matter effecting AOU demands of the Arctic Ocean. *Prog. Oceanogr.* **22**, 277–359.

Whitledge, T. E., Bidigare, R. R., Zeeman, S. I., Sambrotto, R. N., Roscigno, P. F., Jensen, P. R., Brooks, J. M., Trees, C. and Veidt, D. M. 1988. Biological measurements and related chemical features in Soviet and United States regions of the Bering Sea. *Cont. Shelf Res.* **8**, 1299–1319.